forests

MDPI

Article

Structural Monitoring of a Large Archaeological Wooden Structure in Real Time, Post PEG Treatment

Hugh Collett [1,*], Florian Bouville [1], Finn Giuliani [1] and Eleanor Schofield [2,*]

[1] Department of Materials Science & Engineering, Imperial College London, Kensington, London SW7 2AZ, UK; f.bouville@imperial.ac.uk (F.B.); f.giuliani@imperial.ac.uk (F.G.)
[2] Mary Rose Trust, College Road, HM Naval Base, Portsmouth PO1 3LX, UK
* Correspondence: h.collett19@imperial.ac.uk (H.C.); e.schofield@maryrose.org (E.S.)

Abstract: Large archaeological wooden structures are potentially at risk of structural failure through deformation and cracking over time if they are left untreated and their structural health is not maintained. This could be in part due to, for example, the shrinkage of waterlogged wood as it dries, or time-dependent creep processes. These dimensional changes are accompanied by associated stresses. However, there are few studies analysing the movement of large wooden structures in real time as they dry, particularly after their conservation treatment. This paper follows the structural monitoring of the *Mary Rose* from after the conservation treatment, where it was sprayed with polyethylene glycol, through to the ship's air-drying process and beyond to assess the effects that drying has had on the displacement of the timbers. A laser-based target system was used to collect displacement data between 2013 and 2020 and the data showed a significant slowing of displacement as the drying reached an equilibrium.

Keywords: archaeological wooden structures; structural analysis; geodetic systems; drying process; polyethylene glycol

Citation: Collett, H.; Bouville, F.; Giuliani, F.; Schofield, E. Structural Monitoring of a Large Archaeological Wooden Structure in Real Time, Post PEG Treatment. *Forests* **2021**, *12*, 1788. https://doi.org/10.3390/f12121788

Academic Editors: Magdalena Broda and Callum A. S. Hill

Received: 19 October 2021
Accepted: 9 December 2021
Published: 16 December 2021

1. Introduction

Wood has been used as material for building, furniture and ship construction for thousands of years [1–3]. The fact that it is still one of the most widely used building materials is a testament to its suitability and abundance. As a result, there are examples of extant large archaeological wooden structures that we have been able to rediscover/preserve centuries later. Some of these have been discovered underwater, trapped in soil or silt that prevented their degradation over the years [4].

Evaluating the properties and predicting the dimensional change and movement during the drying of large archaeological wooden structures is very challenging for a number of reasons. Firstly, the properties of archaeological wood depend on multiple conditions, including age, wood species, use and the conditions the artefact has been buried in. Large structures may also be composed of wood from several different trees. Secondly, wood is an anisotropic and heterogeneous material [5]. Properties vary within the same piece and with different orientations. The properties of wood and its response to load vary over time and are dependent on the amount of degradation and any changes in moisture content [6]. Finally, to ensure the long-term stability of the structure, a conservation process is generally carried out. This aims to compensate for lost material, achieve dimensional stability and reduce shrinkage of the marine archaeological wood during drying. This process alters the chemical composition and mechanical properties of the wood, adding to the complexity of understanding it.

Previous research studies provide us with an understanding of how changes in moisture content affect the properties and dimensions of large archaeological wooden structures [7,8]. However, there are very few studies into the structural changes that occur in large archaeological wooden objects in real time as they reach their drying equilibrium.

Wood is hygroscopic and the moisture content of archaeological oak can be as high as approximately 700%, with the loss of wood substance as high as approximately 80%, a key indicator of degradation [9]. The moisture content of wood is defined as the ratio of the total mass of moisture within the wood to the mass of the dry wood, and hence moisture contents of wood that are greater than 100% are possible. After removal from the burial site, the migration of moisture during drying can thus cause severe dimensional changes [10]. In anaerobic conditions, wood can survive for thousands of years due to limited degradation because of the reduced development of decay fungi [11]. Once extracted, however, these structures need to be dried, which, if not performed properly, can lead to cracking due to the shrinkage associated with the removal of water, and the voids created by degradation [12].

There are several different methods for stabilising recovered waterlogged archaeological wooden objects [13]. Older, obsolete treatments, such as the application of alum salts, suffer from severe deterioration [14]. Polyethylene glycol (PEG) impregnation is still the most common treatment for conserving waterlogged archaeological wood. The advantages of PEG are its low cost and straightforward methodology [15]. However, we do now know that PEG can cause issues for the wood, e.g., acid production and creep [16].

An important example of a PEG-treated, large archaeological wooden ship is the *Mary Rose*, which will be the focus of this study. The *Mary Rose* is the oldest extant Tudor warship and was the flagship of Henry VIII's fleet. The ship was sunk in 1545 and raised from the seabed 437 years later in 1982. Between 1994 and 2004 the ship was sprayed with low molecular PEG 200, which was administered in an aqueous solution with concentration levels of up to 40%. The PEG concentration was increased incrementally in 5–10% increments. From 2004 until April 2013, the ship was sprayed with higher concentrations of high molecular PEG 2000. Immediately after spraying was completed, the ship's environment was controlled at 50–58% relative humidity with temperatures of 18–20 °C, which has been kept consistent ever since [17]. The moisture content of sections of the ship has been determined using the gravimetric method since the spraying was ceased. The analysis has shown that the ship is now predominantly dry and that only limited movement due to drying should now be occurring [18]. Moisture content studies have been carried out since the onset of drying, but, due to the high variability of wood, there is corresponding variability in the moisture content value as a function of depth and location around the hull. However, in 2016, the surface in all of the locations studied on the ship was found to have a moisture content below 15%, and core samples displayed a MC% of between 10–20% [18]. It was therefore at this point determined to be predominantly dry, with only minimal moisture left to migrate out.

As discussed, large archaeological wooden structures, such as the *Mary Rose*, are complex to monitor and understand. While shrinkage in the direction of the growth ring is generally limited to 7–8% in recent wood, it can be around 60% in deteriorated archaeological wood [19]. This is compounded by the difference in drying shrinkage associated with different species and orientations, and it is complicated to assess the health of large wooden structures and predict changes in their structural integrity. It is, however, possible to measure the displacement and distortion of these large wooden structures in real time during drying to better understand the drying process. The monitoring should also alert the conservator to any major changes that need swift intervention. Non-contact geodetic measurements, such as theodolites, photogrammetry and terrestrial laser scanners, have all been used extensively in cultural heritage [20–22]. Many constraints limit the scanning systems that can be used to obtain the three-dimensional coordinates of the structure in question. These include the size and shape of the object, the surface material of the object (e.g., reflectance) and the cost, ease of use, etc. [23].

This paper analyses the displacement undergone by the *Mary Rose* shipwreck during conservation and the procedure undertaken to collect geodetic measurements of this large wooden structure. As a result of the anaerobic environment of the seabed, the ship remained in good condition. The conservation treatment consisted of spraying with

two molecular weights of polyethylene glycol (PEG) before undergoing a controlled air-drying procedure [24]. The PEG conservation treatment was similar to the treatment of the *Vasa* shipwreck, however there was limited real-time/live monitoring of displacement throughout the *Vasa* drying process [25]. From the geodetic measurements collected continuously over the years, the aim of this study is to analyse the changes in displacement and displacement rate over the years 2013–2020 to identify any major structural changes in the timbers and to provide a greater understanding of the drying process of large wooden structures that are impregnated with PEG. While the displacement analysis will help to identify any immediate and long-term concerns regarding the structural stability of the *Mary Rose*, the findings and methodology will also be applicable to other similar large wooden structures worldwide.

2. Methods and Measuring Systems

The methods section briefly summarises the systems used to monitor displacement at points on the *Mary Rose*'s hull by comparing current positions with a reference point.

A total station (TS), Leica NOVA TS50, Germany, was installed in September 2013 (approximately 4 months after drying commenced) to observe the global and local movements of the ship. The geodetic monitoring system, with an accuracy of 0.6 mm in distance measurements and 0.0001° in angle measurement, is located on the port side. The total station recorded the position of targets on the ship at 08:00, 16:00 and 00:00 every day since late 2013. However, there are some gaps in recordings due to conservation work on the ship during this time.

Total stations work according to the phase-shift principle. A signal is sent from the total station towards the targets and the phase of the returning signal is compared to the phase of the emitted signal. The electromagnetic signals are fired at targets of cooperative materials. A typical total station is able to measure distances of up to 1500 m with an accuracy of 1.5 mm [26]. The total station data are obtained from the machine automatically as X, Y and Z coordinates, and have been processed in Python using a Jupyter Notebook.

The data were processed as follows:

- Errors in the total station data, such as a sudden and constant shift in the Z direction data of more than 10 mm that was stable over a long period of time, were removed. The source of this shift has not been conclusively proven, but is likely to be a hardware error since the recording returned to normal after some time and the oscillation desisted of its own accord.
- For the total displacement plots, a scatter graph was plotted showing the total displacement against time for each target in each direction.
- For the displacement rate plots, a curve of best fit was plotted on each target's dataset. The fitted curve was then differentiated to find the rate of change.

In total there are 35 targets on the ship that are scanned by the total station (c.f., Figure 1) and the name of each target was chosen as follows. The first number increases moving from bow to stern. The second number describes which deck the target is located on: 01 indicates the target is on the orlop deck, 02 indicates the main deck, 03 the upper deck and 04 the castle deck. Taking the target labelled 01.01 as an example, the first 01 denotes that the target is the closest to the bow on that deck. The second 01 indicates that the target is located on the orlop deck.

The X direction is positive from stern to bow. The Y direction is positive from port to starboard and the Z direction is positive from the ground up.

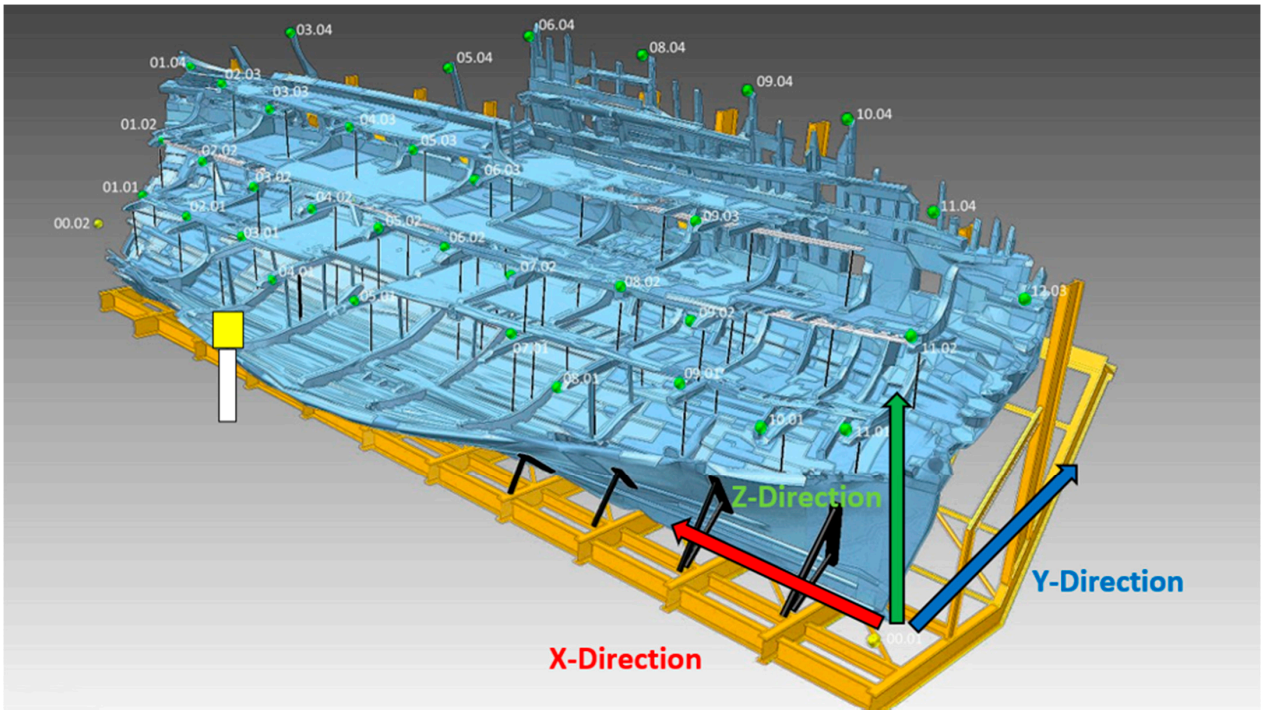

Figure 1. Schematic of the *Mary Rose* showing the location of the laser targets on the ship and the laser scanner.

3. Results and Discussion

3.1. Total Displacement of the TS Targets in the X, Y and Z Directions Respresented on the Ship

The position of each target on the ship and the displacement measured from the September 2013 to March 2020 is shown in Figure 2. The green arrows are proportional to the displacement's magnitude in the Z direction, the blue arrows the Y direction and the red arrows the X direction. One conclusion that can be drawn from this Figure is that the displacement increases moving higher up the ship. For instance, the average X, Y and Z displacement in the orlop deck is 60 mm, 20 mm and 40 mm, respectively, whereas, in the castle deck the values are 55 mm, 140 mm and 180 mm, respectively.

Focusing on the Z direction, the whole ship experienced downward displacement, as would be expected. The Z displacement is around 1.3, 2.2 and 4.3 times larger on average in the castle deck than in the upper, main, and orlop decks, respectively. This is the effect of the cumulative deformation of the decks below. In addition, the castle deck has the least support and the targets are attached to more independent sections of wood, as opposed to the beams in the lower sections that are more interconnected with the original ship structure and which had subsequent supports installed.

The displacement along the Y direction is predominantly from starboard to port throughout, i.e., negative. In contrast, the displacement along the X direction switches on alternate decks, creating a shear-like movement. The largest displacements in any one direction are approximately 250 mm. These occurred in the castle deck in the Y and Z directions and only in two targets.

3.2. Cumulative Displacement of the TS Targets in the X, Y and Z Directions over the Time Period (2013–2020)

By looking at the displacement of each deck separately over time, we found that the movement of the majority of the positions was slowing down over time, independent of direction. Figure 3 displays the displacement along the X direction over time between September 2013 (Year 0) and March 2020 (Year 6.5). The few positions where the rate of displacement was near constant over the time period of September 2013–March 2020 were displacing at a slow rate.

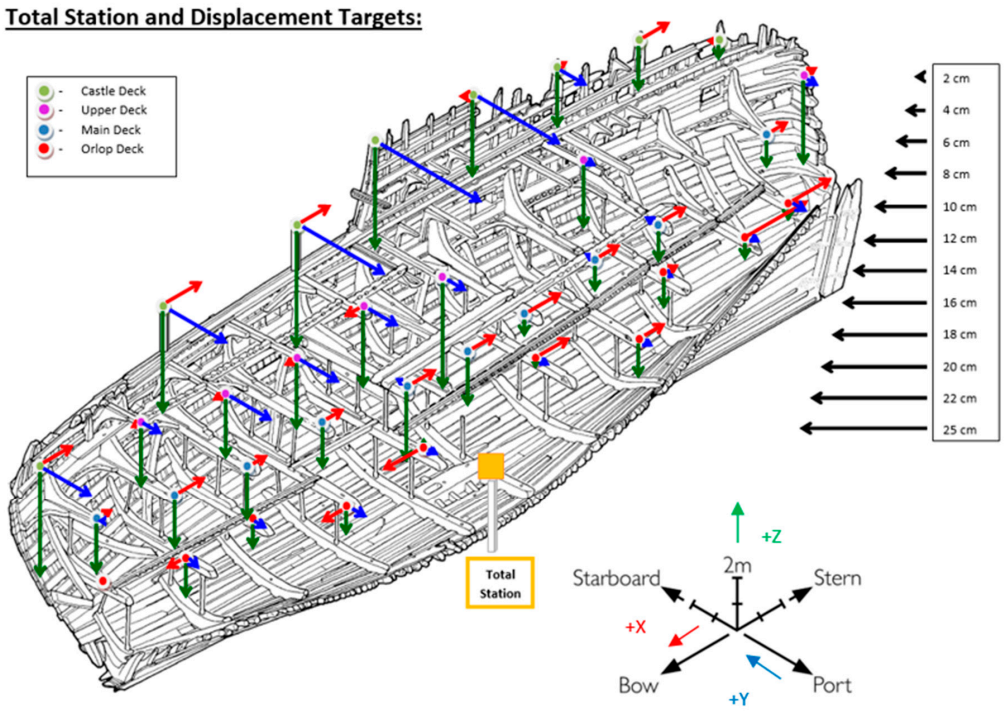

Figure 2. Shows the total displacement of the targets between 2013 and 2020 in the X (red arrows), Y (blue arrows) and Z (green arrows) directions. The scale bar on the right is a reference for the magnitude of the displacements.

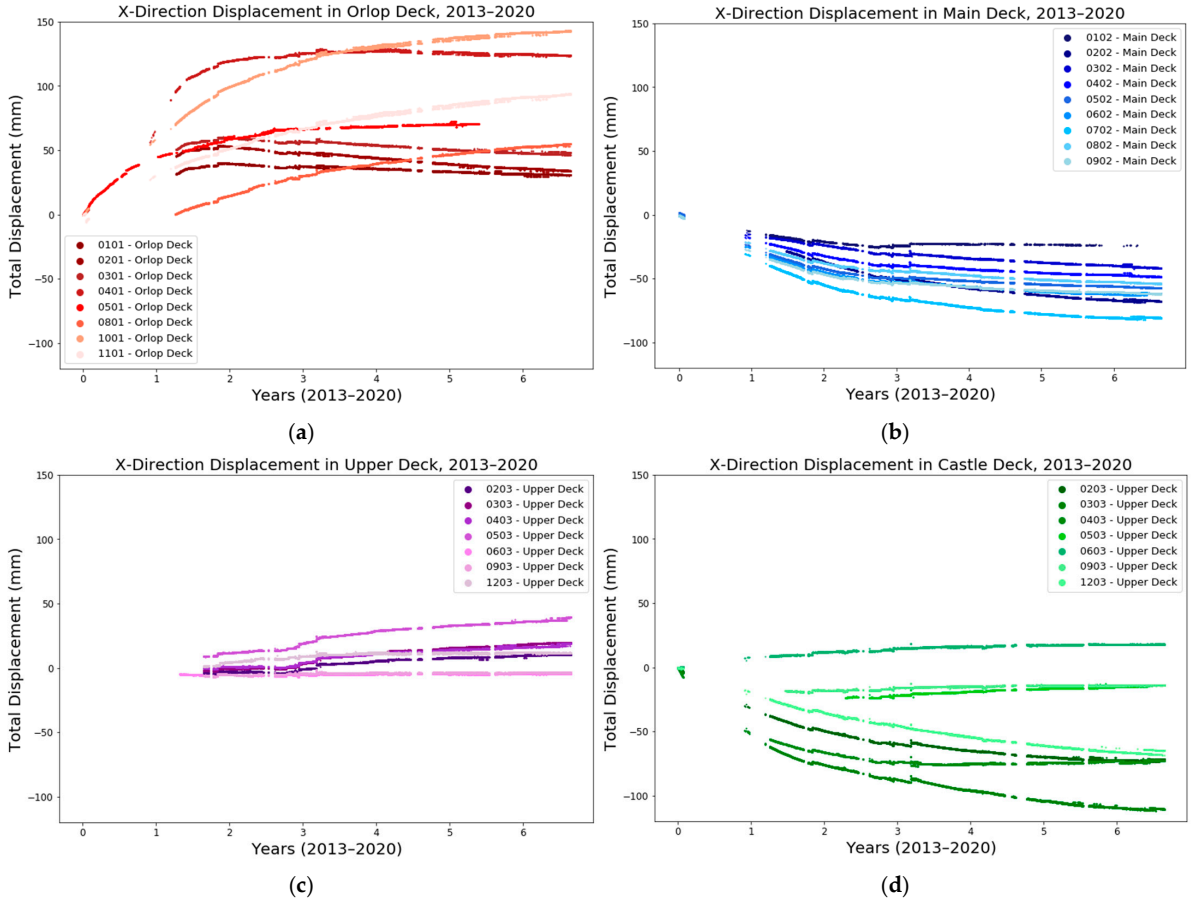

Figure 3. X direction displacement of the TS targets in the (**a**) orlop, (**b**) main, (**c**) upper and (**d**) castle decks plotted against time for the period between September 2013 and March 2020.

The displacement along the X direction in the ship experienced a concertina motion as the direction of the displacement flipped between each deck. The direction of displacement in the X direction is consistent across each deck, with an average of +60 ± 40 mm for the orlop deck, +20 ± 9 mm for the upper deck, −60 ± 20 mm for the main deck and −60 ± 30 mm for the castle deck. The orlop deck and the castle deck have displaced further than the main and upper decks. This is potentially because the orlop deck does not have the titanium support beams that the other decks have, and the castle level is the least interconnected.

Displacement in the Y direction is shown in Figure 4. The displacement along Y averaged at approximately −20 ± 10 mm in the orlop deck, +10 ± 10 mm in the main deck, −60 ± 30 mm in the upper deck and −150 ± 80 mm in the castle deck. The target with the greatest displacement between 2013 and 2020 is the 06.04 target, towards the centre of the castle deck, which has displaced by 250 mm.

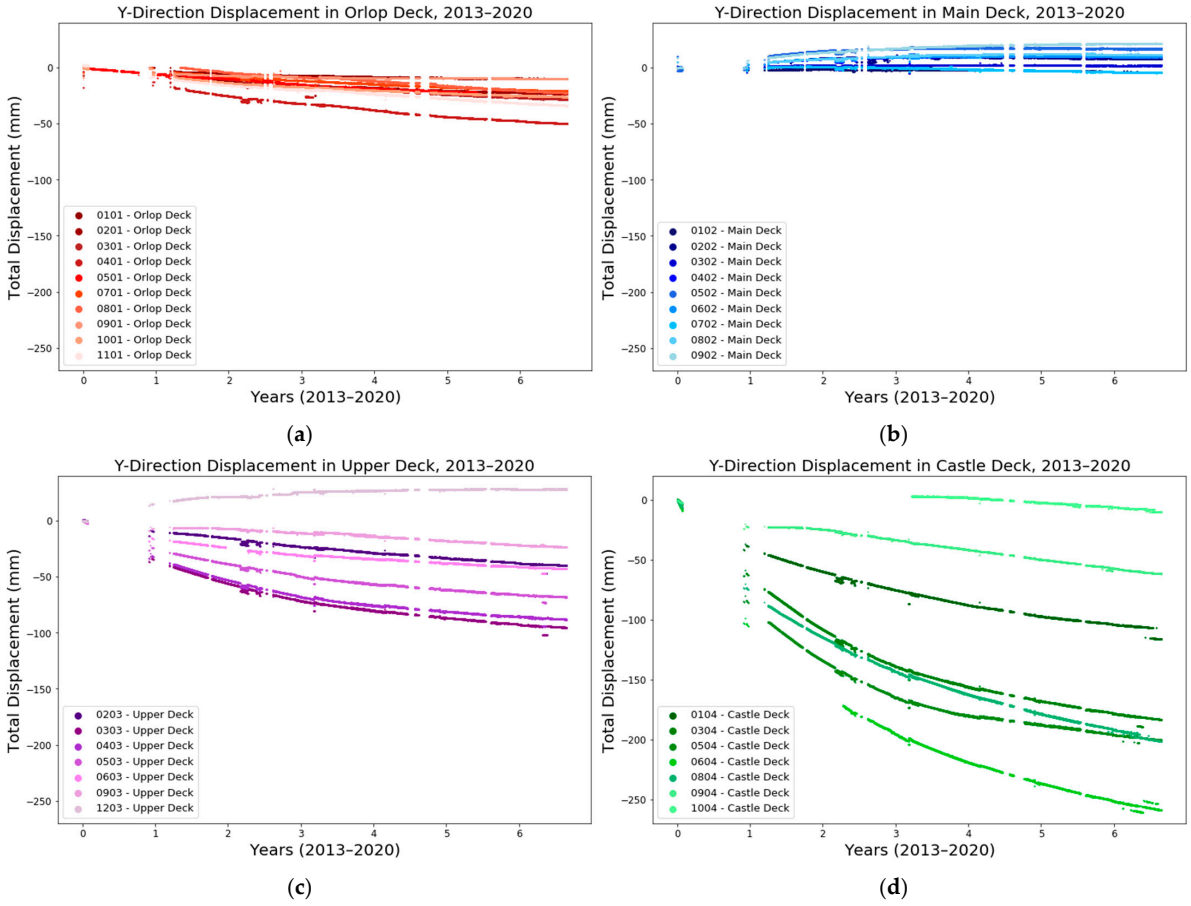

Figure 4. Y direction displacement of the TS targets in the (**a**) orlop, (**b**) main, (**c**) upper and (**d**) castle decks plotted against time for the period between September 2013 and March 2020.

Similarly to the displacement along the X direction, some targets display negative Y displacement and some positive, i.e., some targets were displaced from starboard to port and others port to starboard (c.f., Figure 2). This could create a shearing motion in the ship, although the majority of Y displacement is from starboard to port. In total, 26 of the targets moved in the negative Y direction and eight in the positive direction. The sum of total negative displacement of all the targets in the Y direction is 1500 mm, whereas the total movement in the positive Y direction, i.e., from port to starboard, is 170 mm. The targets were displaced far more from starboard to port than port to starboard.

Comparisons across the four decks in Figure 5 show that the total displacement in the Z direction increased in each higher deck. The average displacement in the Z direction

in the orlop deck was -40 ± 20 mm, in the main deck it was -90 ± 30 mm, in the upper deck it was -150 ± 30 mm and in the castle deck it was -190 ± 50 mm. The greatest total displacement of 260 mm occurred in the castle deck. This means that the 05.04 target, which is around halfway along the castle deck of the ship (c.f., Figure 2), has displaced more than any other target in the Z direction.

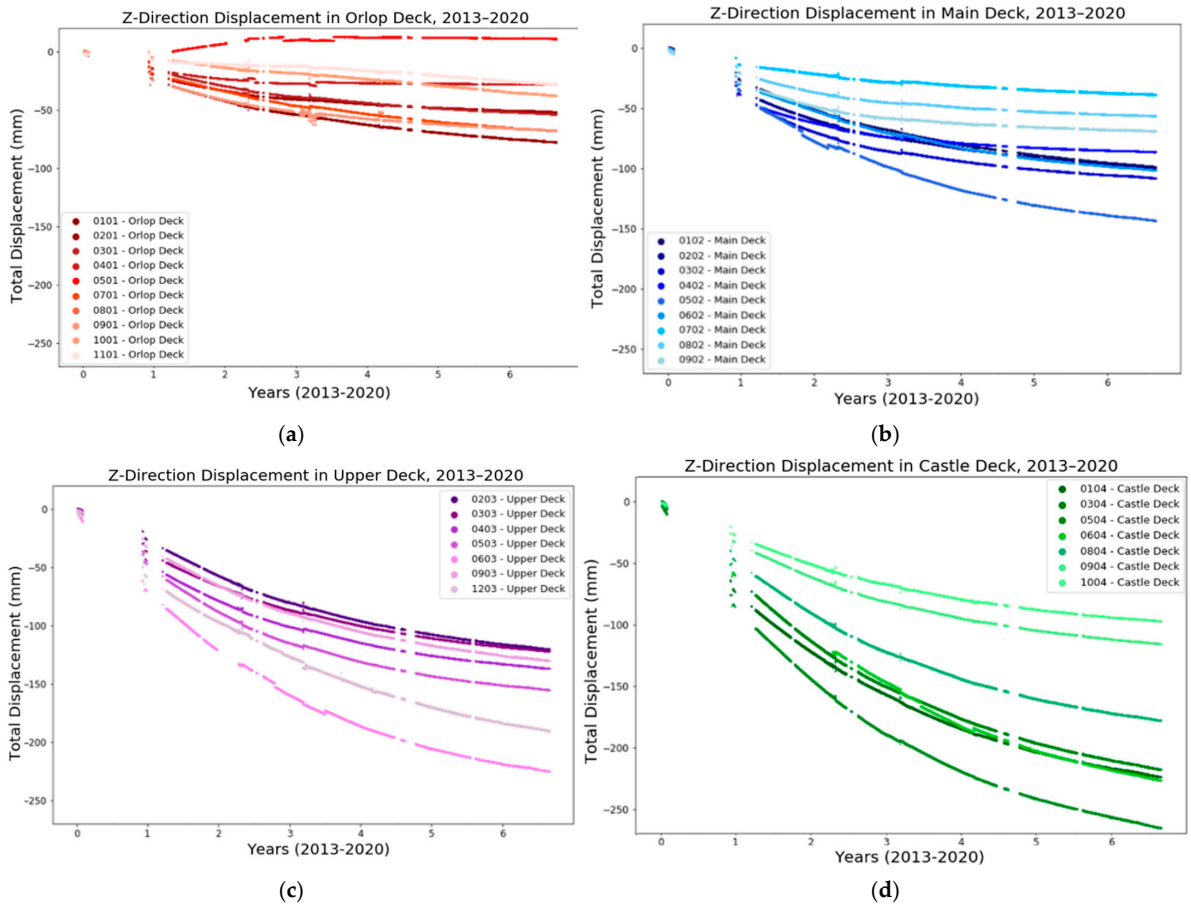

Figure 5. Z direction displacement of the TS targets in the (**a**) orlop, (**b**) main, (**c**) upper and (**d**) castle decks plotted against time for the period between September 2013 and March 2020.

Unlike the trends moving up the ship's decks in the Z direction, the trends moving across the ship from stern to bow are less clear. However, the largest displacement in each deck occurred in the targets 02.01, 05.02, 06.03 and 06.04. From this, one conclusion could be that the Z displacement is greatest in the middle of the ship, i.e., a relatively equal distance between bow and stern.

Fortunately, all the targets slowed in their displacement, as evidenced by the decay in magnitude for all of the displacements measured, regardless of the direction and position on the ship.

3.3. Displacement Rate of the TS Targets in the X, Y and Z Directions over the Time Period (2013–2020)

Notable amongst the X direction displacement rate plots in Figure 6, the 04.01 target displayed a high initial rate of 165 mm/year in the first 2 weeks of recording. However, the rate of displacement for this target slowed to a similar level to all other targets after the first year. The issue with the 04.01 target can be explained by the damage to the hull at the point where this target was attached, which had to be repaired in November 2013, with scaffolding support being inserted. This was then reinforced up to the main deck in September 2014.

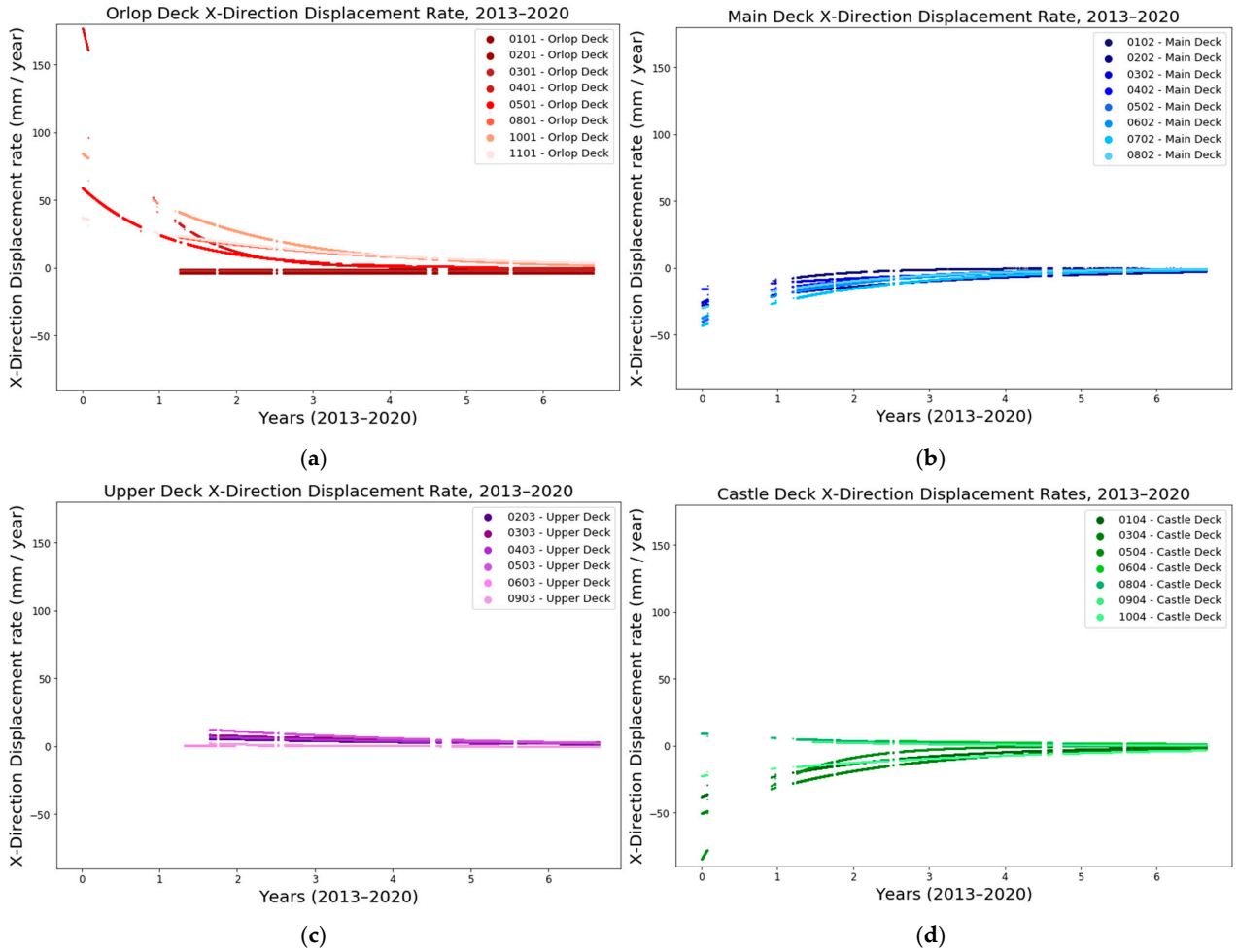

Figure 6. Rate of the X displacement of the TS targets in the (**a**) orlop, (**b**) main, (**c**) upper and (**d**) castle decks plotted against time for the period between September 2013 and March 2020.

The most recent X direction displacement rates are similar, and relatively slow, across the four decks and across the length of the ship, too, with an average of +2 ± 1 mm/year in the orlop deck, −1.0 ± 0.6 mm/year in the main deck, +2.0 ± 1.6 mm/year in the upper deck and 1 ± 1 mm/year in the castle deck. The displacement rates across all targets show promising signs of slowing in the X direction.

The Y displacement rates in Figure 7 show a similar pattern of slowing as they do along the X direction. While there was some variance of the initial displacement rate, with the value going from 110 mm/year in the fastest displacing target in 2013, which was 06.04, as of 2020, all the displacement rate magnitudes were below 20 mm/year. For instance, 06.04 was approximately 110 mm/year and, as of 2020, was approximately 7 mm/year, whereas the 09.04 target was approximately 8 mm/year and became 7 mm/year.

The average most recent Y direction displacement rates are 2 ± 1 mm/year in the orlop deck, 0.2 ± 0.2 mm/year in the main deck, 3 ± 1 mm/year in the upper deck and 5 ± 2 mm/year in the castle deck. The most recent average rate of X direction displacement is highest in the castle deck.

Figure 8 presents the displacement rates along the Z direction of the targets in each separate deck. Similarly to the two other directions, the rate of displacement was reducing in all targets over the 6.5 years since September 2013.

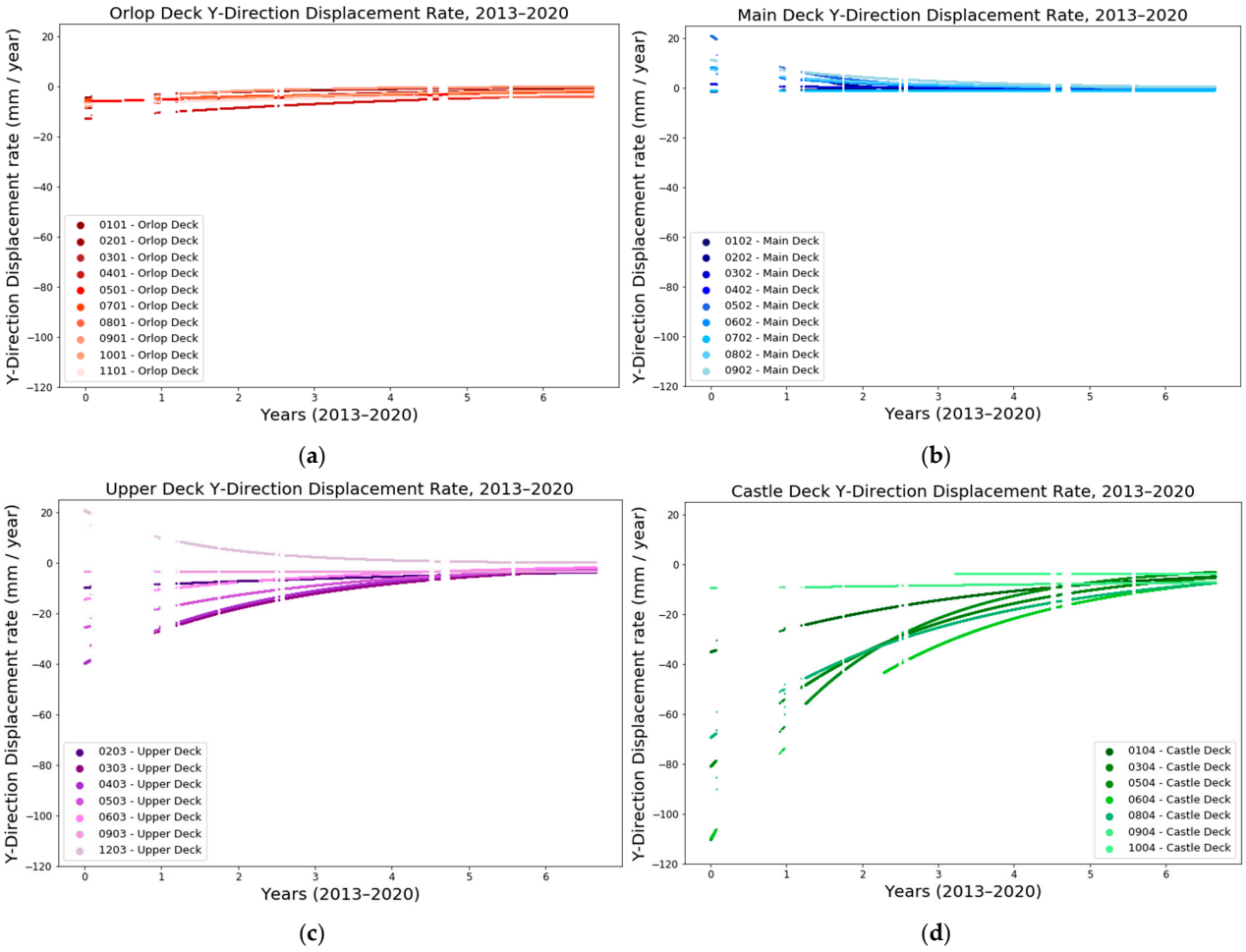

Figure 7. Rate of the Y displacement of the TS targets in the (**a**) orlop, (**b**) main, (**c**) upper and (**d**) castle decks plotted against time for the period between September 2013 and March 2020.

The faster initial rates of displacement of the upper and castle decks could be expected from the discussion in the previous total displacement section. The most recent displacement rates are still higher in the upper decks, even though they have reduced and are now all below 20 mm/year.

The most recent average displacement rates in the Z direction for targets in each deck are: 2 ± 2 mm/year in the orlop deck, 3 ± 2 mm/year in the main deck, 7 ± 2 mm/year in the upper deck and 9 ± 3 mm/year in the castle deck. If the targets continue to follow the same Z displacement trends, then the Z displacement rates should approach zero.

The most recent rates of displacement of each target are shown in Figure 9a–c. The ship is currently moving most in the Z direction across all four decks. In addition, the most recent displacement rate is highest in the upper two decks and increases moving up the ship. Since the ship is predominantly dry, according to the moisture content recordings, the most recent limited movement is from other structural considerations, such as interconnectivity, or lack of, within the ship.

As a rough selection process for identifying problematic sections, we could investigate any targets currently displacing faster than 10 mm/year. From the graphs, the sections with greater than 10 mm/year displacement are 03.04, 05.04 and 06.04. These should be monitored carefully moving forward to ascertain if they will slow down in accordance with the other sections.

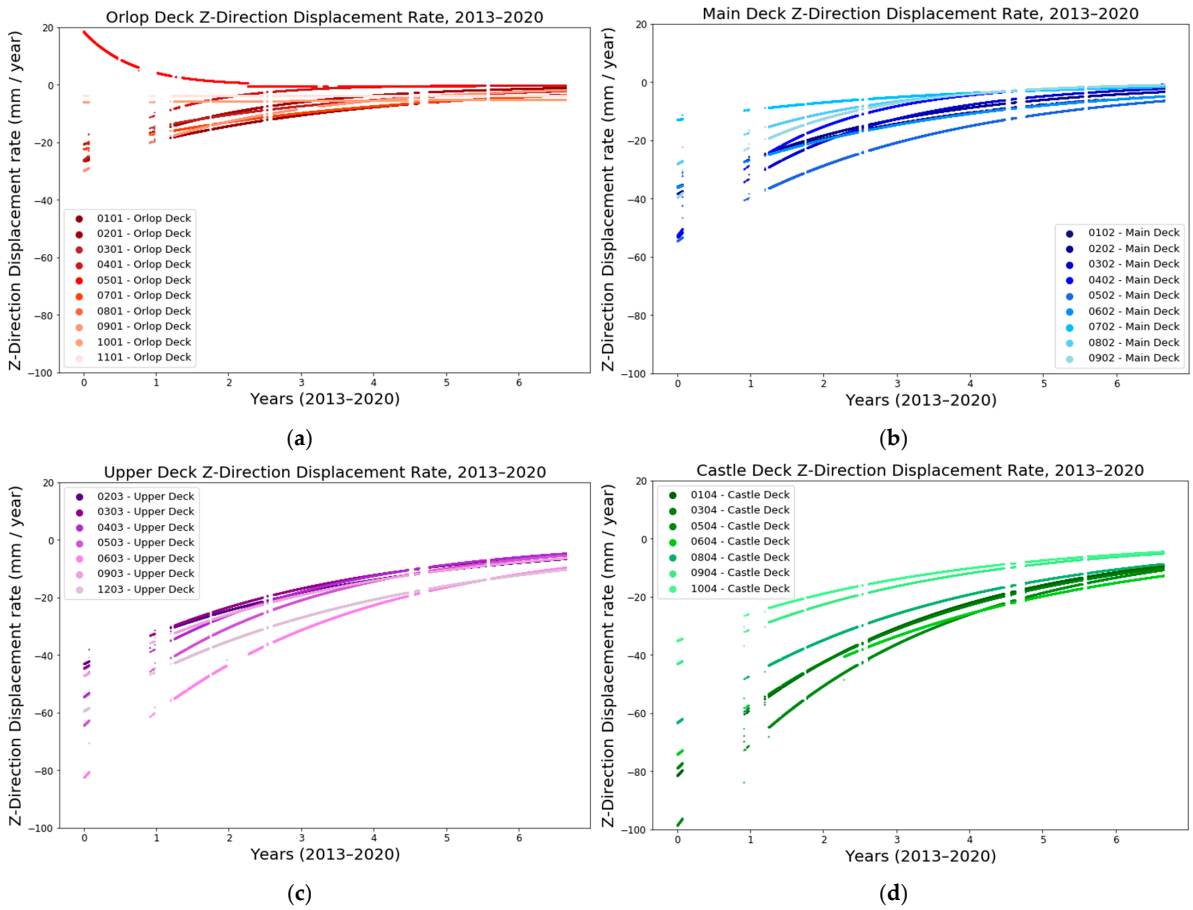

Figure 8. Rate of the Z displacement of the TS targets in the (**a**) orlop, (**b**) main, (**c**) upper and (**d**) castle decks plotted against time for the period between September 2013 and March 2020.

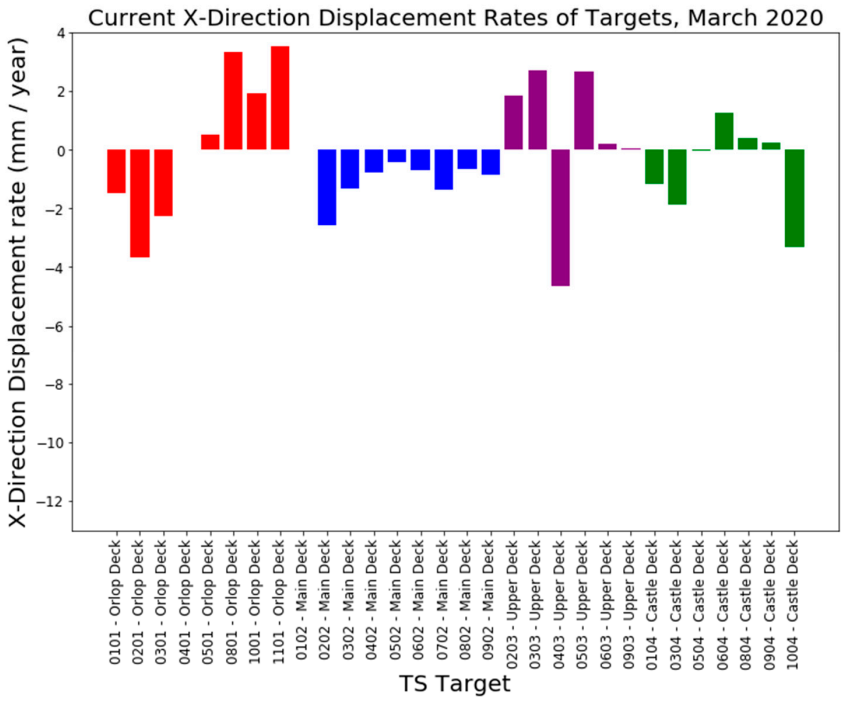

Figure 9. *Cont.*

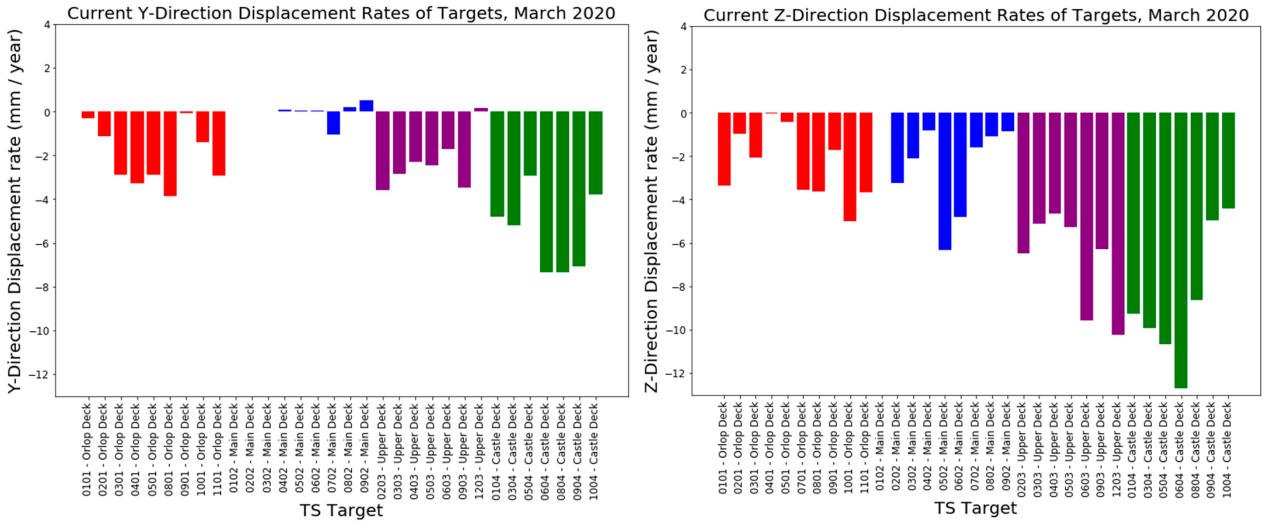

(**b**) (**c**)

Figure 9. Most recent (2020) displacement rates in the (**a**) X, (**b**), Y and (**c**) Z directions. The colour of the bars denotes the deck on which the target is located: red—orlop, blue—main, purple—upper, green—castle.

4. Conclusions

In this study on the *Mary Rose*, we've illustrated how a laser-based target system can be used to measure the displacement of a large archaeological wooden structure, in real time, during the air-drying process after PEG treatment. The displacements since the drying process began were significant in the early stage of drying, but have since slowed considerably.

- In the first year of drying, in the X, Y and Z directions, the highest displacement rates were 70, 110 and 100 mm/year, respectively, whereas after 6.5 years the highest displacement rates are an order of magnitude slower, at 5, 7 and 12 mm/year respectively. Evidently, the displacement rates have reduced significantly, which is a positive finding, indicating the stabilisation of the hull.
- This slower rate of displacement corresponds to an average displacement of the targets in the X, Y and Z directions between the period of recording (2013–2020) of approximately 50, 60 and 110 mm, respectively.
- Average displacement rates as of 2020 across all targets in the X, Y and Z directions are approximately 1.6, 2.3 and 5 mm/year respectively. The displacement rates are now reasonably small when considered in context of the approximately 30 m long ship.
- Finally, as a first analysis of current displacement rates to identify critical sections in need of intervention, the work conducted here alleviates any fears of significant further displacement.

Author Contributions: Conceptualization, E.S., F.B., F.G. and H.C.; methodology, E.S., F.B., F.G. and H.C.; software, E.S.; validation, E.S.; formal analysis, E.S., F.B., F.G. and H.C.; investigation, E.S., F.B., F.G. and H.C.; resources, H.C.; data curation, E.S., F.B., F.G. and H.C.; writing—original draft preparation, E.S., F.B., F.G. and H.C.; writing—review and editing, E.S., F.B., F.G. and H.C.; visualization, H.C., E.S., F.B. and F.G.; supervision, E.S., F.B., F.G. All authors have read and agreed to the published version of the manuscript.

Funding: H.C. received funding for a Ph.D. by the EPSRC Centre for Doctoral Training in the Advanced Characterisation of Materials (CDT-ACM)(EP/L015277/1).

Institutional Review Board Statement: Not applicable.

Informed Consent Statement: Not applicable.

Data Availability Statement: Not applicable.

Conflicts of Interest: The authors declare no conflict of interest.

References

1. Varga, T.; Pauliny, P. Timber-traditional material history or vision in architectural design? In *Advanced Materials Research*; Trans Tech Publications Ltd.: Freienbach, Switzerland, 2014; Volume 899, pp. 460–465.
2. Namichev, P.; Petrovski, M. Wood as a primary selection of material for furniture production. *J. Process. Manag. New Technol.* **2019**, *7*, 6–12. [CrossRef]
3. Laures, F.F. The evolution of antique ship construction in the Mediterranean: A hypothesis. *Int. J. Naut. Archaeol.* **1984**, *13*, 323–325. [CrossRef]
4. Majka, J.; Zborowska, M.; Fejfer, M.; Waliszewska, B.; Olek, W. Dimensional stability and hygroscopic properties of PEG treated irregularly degraded waterlogged Scots pine wood. *J. Cult. Herit.* **2018**, *31*, 133–140. [CrossRef]
5. Eriksen, A.M.; Gregory, D.J.; Villa, C.; Lynnerup, N.; Botfeldt, K.B.; Rasmussen, A.R. The effects of wood anisotropy on the mode of attack by the woodborer Teredo navalis and the implications for underwater cultural heritage. *Int. Biodeterior. Biodegrad.* **2016**, *107*, 117–122. [CrossRef]
6. Nagao, K.; Fujii, S. Effect of Moisture Content and Temperature on the Mechanical Properties of Food Models for Examining Thermal Conduction. *J. Home Econ. Jpn.* **2004**, *55*, 573–580.
7. Vorobyev, A.; van Dijk, N.P.; Gamstedt, E.K. Orthotropic creep in polyethylene glycol impregnated archaeological oak from the Vasa ship: Results of creep experiments in a museum-like climate. *Mech. Time-Depend. Mater.* **2019**, *23*, 35–52. [CrossRef]
8. Dionisi-Vici, P.; Allegretti, O.; Braovac, S.; Hjulstad, G.; Jensen, M.; Storbekk, E. The Oseberg ship. Long-term physical-mechanical monitoring in an uncontrolled relative humidity exhibition environment. Analytical results and hygromechanical modelling. In Proceedings of the Climate for Collections Standards and Uncertainties, Munich, Germany, 7–9 November 2012.
9. Broda, M.; Mazela, B.; Królikowska-Pataraja, K.; Hill, C.A.S. The use of FT-IR and computed tomography non-destructive technique for waterlogged wood characterisation. *Wood Res.* **2015**, *60*, 707–722.
10. Thybring, E.E.; Glass, S.V.; Zelinka, S.L. Kinetics of water vapor sorption in wood cell walls: State of the art and research needs. *Forests* **2019**, *10*, 704. [CrossRef]
11. Björdal, C.G.; Nilsson, T. Waterlogged archaeological wood—A substrate for white rot fungi during drainage of wetlands. *Int. Biodeterior. Biodegrad.* **2002**, *50*, 17–23. [CrossRef]
12. Kowalczuk, J.; Rachocki, A.; Broda, M.; Mazela, B.; Ormondroyd, G.A.; Tritt-Goc, J. Conservation process of archaeological waterlogged wood studied by spectroscopy and gradient NMR methods. *Wood Sci. Technol.* **2019**, *53*, 1207–1222. [CrossRef]
13. Broda, M.; Hill, C.A.S. Conservation of waterlogged wood—Past, present and future perspectives. *Forests* **2021**, *12*, 1193. [CrossRef]
14. McQueen, C.M.A.; Steindal, C.C.; Narygina, O.; Braovac, S. Temperature- and humidity-induced changes in alum-treated wood: A qualitative X-ray diffraction study. *Herit. Sci.* **2018**, *6*, 1–11. [CrossRef]
15. Wagner, L.; Almkvist, G.; Bader, T.K.; Bjurhager, I.; Rautkari, L.; Gamstedt, E.K. The influence of chemical degradation and polyethylene glycol on moisture-dependent cell wall properties of archeological wooden objects: A case study of the Vasa shipwreck. *Wood Sci. Technol.* **2016**, *50*, 1103–1123. [CrossRef]
16. Preston, J.; Smith, A.D.; Schofield, E.J.; Chadwick, A.V.; Jones, M.A.; Watts, J.E.M. The effects of Mary Rose conservation treatment on iron oxidation processes and microbial communities contributing to acid production in marine archaeological timbers. *PLoS ONE* **2014**, *9*, e84169. [CrossRef] [PubMed]
17. Jones, M.; Schofield, E.J.; McConnachie, G. Air drying of the Mary Rose hull'. In Proceedings of the 12th ICOM-CC Group on Wet Organic Archaeological Materials Conference, Istanbul, Turkey, 13–17 May 2013.
18. Piva, E. *Conservation of a Tudor Warship: Investigating the Timbers of the Mary Rose*; Portsmouth University: Portsmouth, UK, 2017.
19. Nguyen, T.D.; Sakakibara, K.; Imai, T.; Tsujii, Y.; Kohdzuma, Y.; Sugiyama, J. Shrinkage and swelling behavior of archaeological waterlogged wood preserved with slightly crosslinked sodium polyacrylate. *J. Wood Sci.* **2018**, *64*, 294–300. [CrossRef]
20. El-Hakim, S.; Beraldin, J.-A.A.; Picard, M.; Cournoyer, L. Surface Reconstruction of Large Complex Structures from Mixed Range Data—The Erechtheion Experience. *Int. Arch. Photogramm. Remote Sens. Spat. Inf. Sci.* **2008**, *37*, 1077–1082. Available online: https://www.researchgate.net/profile/J-A_Beraldin/publication/44054006_Surface_Reconstruction_of_Large_Complex_Structures_from_Mixed_Range_Data_-_The_Erechtheion_Experience/links/00463521d20bbbe45e000000/Surface-Reconstruction-of-Large-Complex-Structures- (accessed on 20 September 2021).
21. Neubauer, W.; Doneus, M.; Studnicka, N.; Riegl, J.; Systems, L.M.; Documentation, D. Combined High Resolution Laser Scanning and Photogrammetrical Documentation of the Pyramids at Giza. *Security* **2005**, 470–475.
22. Vorobyev, A.; Garnier, F.; van Dijk, N.P.; Hagman, O.; Gamstedt, E.K. Evaluation of displacements by means of 3D laser scanning in a mechanically loaded replica of a hull section of the Vasa ship. *Digit. Appl. Archaeol. Cult. Herit.* **2018**, *11*, e00085. [CrossRef]
23. Wujanz, D.; Neitzel, F.; Hebel, H.P.; Linke, J.; Busch, W. Terrestrial radar and laser scanning for deformation monitoring: First steps towards assisted radar scanning. *ISPRS Ann. Photogramm. Remote Sens. Spat. Inf. Sci.* **2013**, *2*, 325–330. [CrossRef]
24. McConnachie, G. *Air Drying Behavior of Waterlogged Archaeological Woods from the Tudor Warship Mary Rose*; Portsmouth University: Portsmouth, UK, 2005.

25. Van Dijk, N.P.; Gamstedt, E.K.; Bjurhager, I. Monitoring archaeological wooden structures: Non-contact measurement systems and interpretation as average strain fields. *J. Cult. Herit.* **2016**, *17*, 102–113. [CrossRef]
26. Leica Flexline TS02/06/09 (Datasheet for model TS06). 2008. Available online: https://leica-geosystems.com/-/media/files/leicageosystems/products/datasheets/leica_viva_ts16_ds.ashx?la=en&hash=2746A736346652C1C8CF15B5371AD534 (accessed on 28 August 2021)